Master of Science

Friction characteristics of two-dimensional hybrid organic-inorganic perovskites at the nanoscale

The Graduate School

of the University of Ulsan

Department of Mechanical Engineering

Hyeseon Park

Friction characteristics of two-dimensional hybrid organic-inorganic perovskites at the nanoscale

Supervisor: Professor Koo-Hyun Chung

A Thesis

Submitted to

the Graduate School of the University of Ulsan

In partial Fulfillment of the Requirements

for the Degree of

Master of Science

by

Hyeseon Park

Department of Mechanical Engineering

University of Ulsan, Korea

December 2020

Friction characteristics of two-dimensional hybrid organic-inorganic perovskites at the nanoscale

This certifies that the master's thesis

of Hyeseon Park is approved.

Committee Chair Prof. Doo-Man Chun

Committee Member Prof. Sung-Tae Hong

Committee Member Prof. Koo-Hyun Chung

Department of Mechanical Engineering

University of Ulsan, Korea

December 2020

CONTENTS

ABSTRACT

Two-dimensional (2D) hybrid organic-inorganic perovskites (HOIPs) have attracted a great deal of interests due to their remarkable photovoltaic properties providing high power conversion efficiency. To achieve reliability for the applications of 2D HOIPs, understanding of friction characteristics is essential. However, the fundamental friction characteristics of 2D HOIPs are not clearly understood yet. Therefore, a more thorough study of friction characteristics of atomically thin 2D HOIPs is needed. In this work, the thickness-dependent friction characteristics of 2D HOIPs were quantitatively investigated using atomic force microscopy (AFM) under various normal forces to determine the frictional behaviors. Three types of 2D HOIPs with different organic chain length were used to investigate the effect of the organic chain length on friction characteristics, and also the effect of the number of layers was examined. The results showed thickness-dependent behavior on the friction characteristics at the nanoscale and the effect of chain length becoming less significant with increasing the number of layers. These results may help to gain a fundamental understanding of friction characteristic of atomically thin 2D HOIPs, so that the results might contribute to broadening their applications.

LIST OF FIGURES

1. INTRODUCTION

1.1. Background and motivation

Hybrid organic-inorganic perovskites (HOIPs) have attracted a great deal of interests as next generation materials in photovoltaic devices field. HOIPs have reached outstanding power conversion efficiency more than 25% in laboratories conditions, which is comparable to thin film solar panels such as commercialized silicon and they could be further improved over 28% if tandem with silicon [1, 2]. Moreover, the production cost of HOIPs is much lower than that of silicon-based solar cells due to the abundant amount on earth and simple scalable solution-based processing method at low temperatures [3]. Additionally, HOIPs also possess remarkable properties as semiconductors such as the tunable direct band gap regardless of the crystal thickness and fast ion migration/orientation under electrical bias [4-6]. Therefore, HOIPs could be applicable to various fields beyond solar cells such as organic light-emitting diodes (OLED), photodetectors, memories, and cathode materials for solid-oxide fuel cells (SOFCs) [7-9].

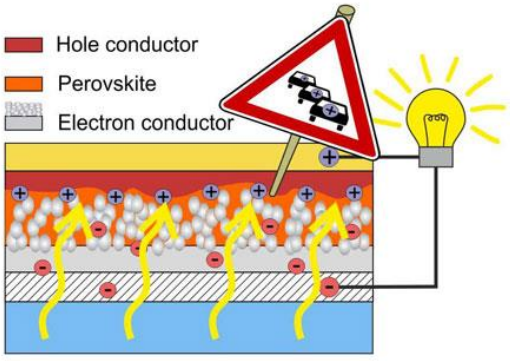

Figure 1. Schematic of the working principle of a perovskite solar cell (S. Weber, 2014).

However, three-dimensional (3D) AMX_3 HOIPs (A = CH_3NH_3, M = Pb, and X = I, Cl, or Br) are vulnerable to heat, oxygen, light irradiation, and moisture due to their poor stability so that they can be easily degraded in the ambient conditions, limiting their applications [10-12]. One of the effective ways to improve the environmental stability is to reduce the dimensionality of 3D HOIPs crystals into layered two-dimensional (2D) HOIPs [13]. In this work, 2D Ruddlesden-Popper family of HOIPs with a general formula of $(R\text{-}NH_3)_2MA_{n-1}Pb_nI_{3n+1}$ were used, where R is the organic spacer molecule, MA is the methylammonium cation, and n indicates the thickness of the inorganic part, and the organic part consists of two adjacent organic layers interfacing each other through van der Waals forces [14-16]. Due to the presence of soft organic layers, 2D HOIPs are among the most compliant materials compared with the other 2D materials and the mechanical properties of 2D HOIPs can be determined by the competition between the stiff inorganic layers, the soft organic layers, and the weak van der Waals interfaces [17].

Given that 2D HOIPs are used as thin films, an understanding of contact surface characteristics such as adhesion and friction is important. Particularly, the nanoscale characteristics are being more important due to miniaturization of electrical devices, hence there are many studies on mechanical energy harvesting technologies that enables sustainable self-powering such as triboelectric nanogenerator (TENG) [18]. As the perovskite serves as not only a triboelectrification material but also a photon-absorbing material in TENG [19], the study on friction characteristics at the nanoscale for improved applicability of 2D HOIPs beyond solar cells is needed. Therefore, this work focused on understanding of friction characteristics to achieve reliability for the applications of 2D

HOIPs. However, the fundamental friction characteristics of atomically thin 2D HOIPs have never been investigated before. Accordingly, a more thorough study of friction characteristics of atomically thin 2D HOIPs is needed.

Since 2D HOIPs are a mixture of organic layers and inorganic layers, the organic chain length is one of the crucial factors determining the performance of solar cells. 2D HOIPs with longer organic chain length possess less surface defects and higher hydrophobicity, resulting in higher power conversion efficiency and long-term durability against moisture [20]. For this reason, it is expected that the organic chain length will also affect the friction properties, so that it is necessary to identify the effect of the organic chain length on friction behaviors for the systematic understanding of the fundamental friction characteristics. Additionally, friction force of atomically thin 2D materials was found to be strongly dependent on the number of layers [21-25], hence the investigation of the effect of the number of layers is also important.

1.2. Objective

This work aims to gain a fundamental understanding of friction characteristics of atomically thin 2D HOIPs at the nanoscale. In this work, the thickness dependent friction characteristics of 2D HOIPs were quantitatively investigated using atomic force microscopy (AFM) under various normal forces to determine the frictional behavior with respect to the organic chain length and the number of layers. Therefore, it can be expected that this work might contribute to broadening the applications of 2D HOIPs by suggesting tunable friction characteristics through controlling the organic chain length or the number of layers.

2. EXPERIMENTAL DETAILS

2.1. Sample preparation and characterization

Three different types of 2D HOIPs were used and they can be expressed with a general formula of $(C_mH_{2m+1}NH_3)_2(CH_3NH_3)_{n-1}Pb_nI_{3n+1}$, where *m* is the number of carbons in the linear organic spacer molecule and *n* indicates the number of inorganic layers. To investigate the effects of the length of the organic spacer molecule, the number of inorganic layers was fixed to one (n = 1) and the number of carbons in the linear organic spacer molecule varied (m = 4, 8, 12) as shown in figure 2 [17]. For the convenience, the type of 2D HOIPs will be expressed as C4, C8, and C12, where the number after C indicates the number of carbon atoms in the organic spacer molecule chain.

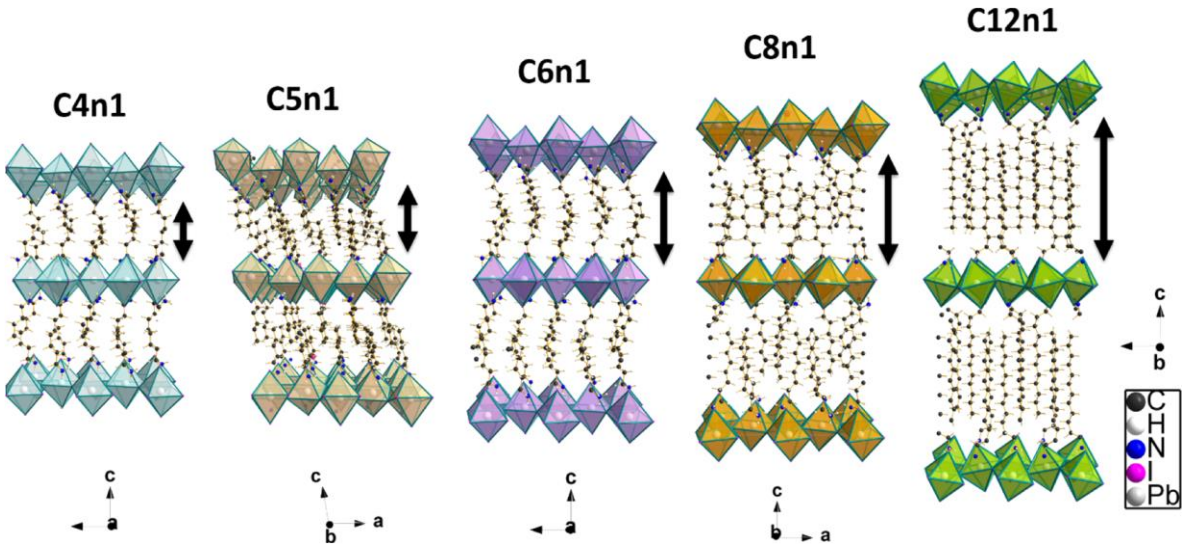

Figure 2. Part of the 2D structures of the layered $(R\text{-}NH_3)_2PbI_4$ materials with increasing length of the organic spacer (R: $CH_3{-}(CH_2)_3{-}$ = C4, $CH_3{-}(CH_2)_4{-}$ = C5, $CH_3{-}(CH_2)_5{-}$ = C6, $CH_3{-}(CH_2)_7{-}$ = C8, and $CH_3{-}(CH_2)_{11}{-}$ = C12) for the same number of inorganic layers, n = 1. The colored octahedra represent the $[PbI_6]^{4-}$

moieties. The black arrow indicates the increase in the distance of the inorganic layers with increasing the length of the organic spacer, ranging from 7.4 to 17 Å [17].

Due to the presence of weak van der Waals interfaces between 2D HOIPs layers, atomically thin 2D HOIPs were deposited onto silicon substrates with 285 nm thick thermally grown SiO_2 by mechanical exfoliation [26, 27] from synthesized single crystal forms. After that, atomically thin 2D HOIPs were located by optical microscopy (VK-X200, Keyence) but their optical contrast on SiO_2/Si substrate was relatively low. Therefore, single-layer 2D HOIPs were randomly located nearby thicker ones, because the optical contrast of atomically thin 2D HOIPs increased as the number of layers increased. Moreover, the number of layers was determined through AFM (Atomic force microscopy, MFP-3D, Asylum Research). To minimize the damage both of 2D HOIPs and AFM tip, topographic images were obtained under the intermittent contact mode using a silicon tip with a nominal spring constant of 2 N/m (AC240, Olympus). Figure 3 shows the topographic images of atomically thin 2D HOIPs along with the cross-sectional height profiles obtained by AFM. Topographic images showed rough surfaces of all types of 2D HOIPs, making it difficult to determine the thickness. In particular, C12 showed different topography from those of C4 and C8 except for the case of bulk, which denotes 2D HOIPs flake with more than 40 layers. Furthermore, based on the cross-sectional height profiles obtained from topographic images, the number of layers was determined as single-layer (1L), bi-layer (2L), tri-layer (3L), quad-layer (4L) and bulk.

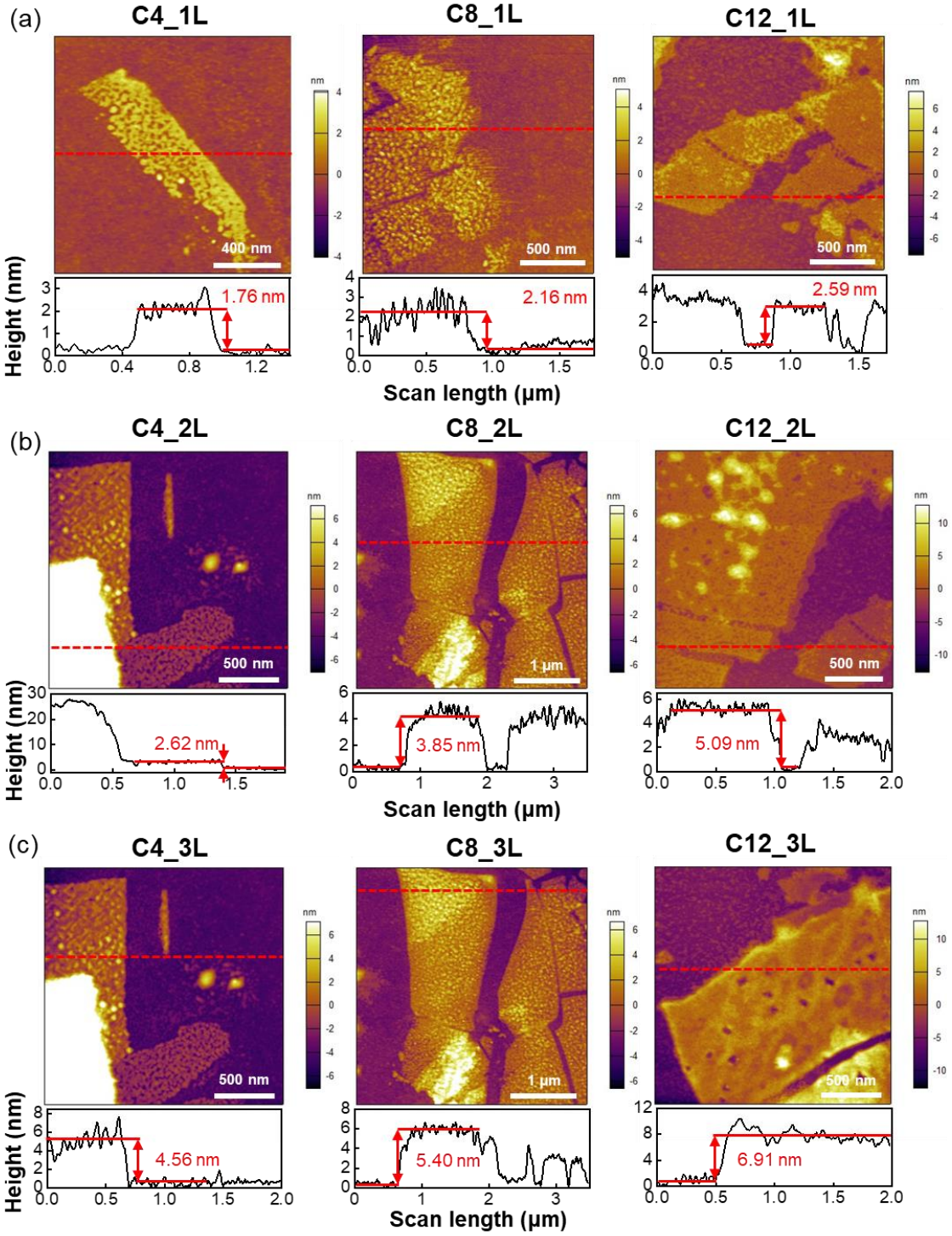
(a)
C4_1L
C8_1L
C12_1L
400 nm
500 nm
500 nm
1.76 nm
2.16 nm
2.59 nm
Height (nm)
Scan length (μm)
(b)
C4_2L
C8_2L
C12_2L
500 nm
1 μm
500 nm
2.62 nm
3.85 nm
5.09 nm
Height (nm)
Scan length (μm)
(c)
C4_3L
C8_3L
C12_3L
500 nm
1 μm
500 nm
4.56 nm
5.40 nm
6.91 nm
Height (nm)
Scan length (μm)

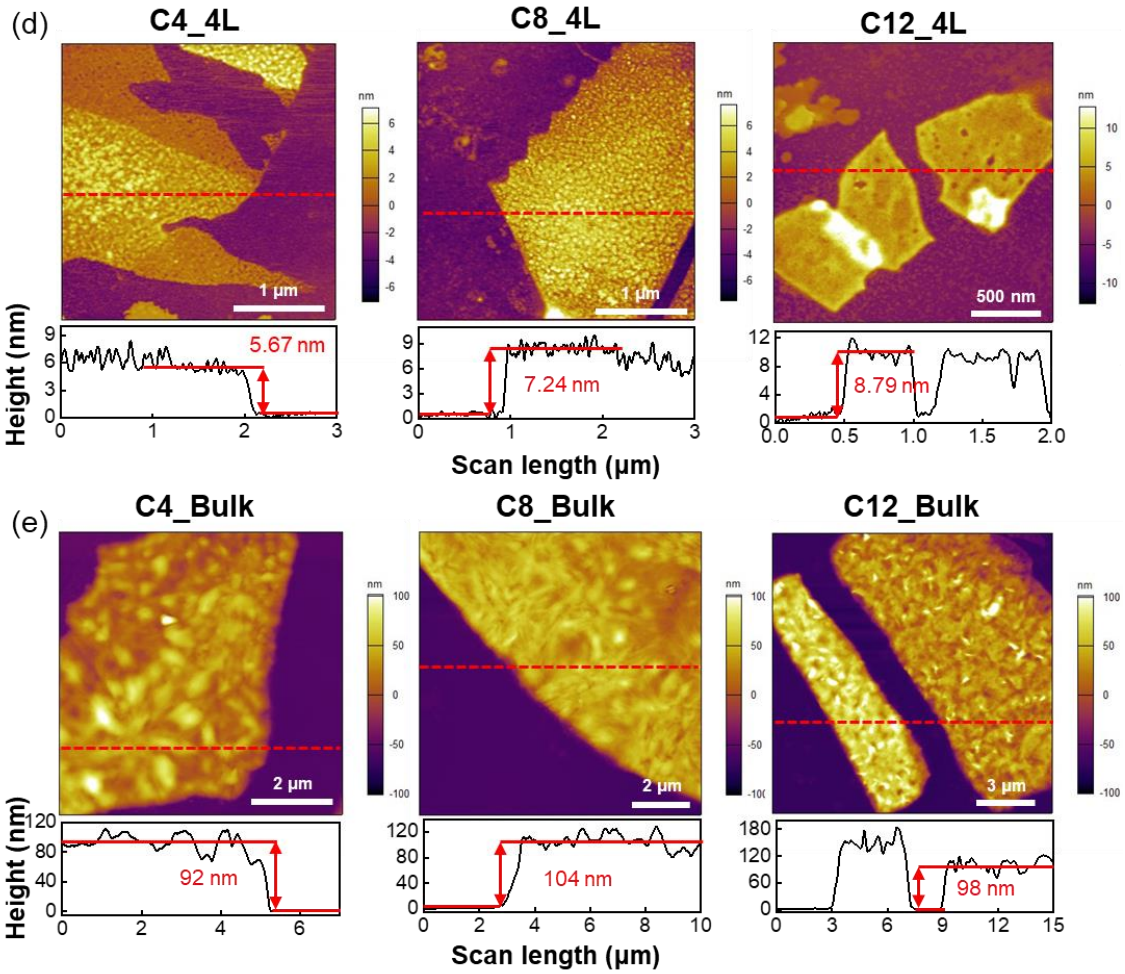

Figure 3. AFM topographic images measured under the intermittent contact mode and cross-sectional height profiles of (a) single-layer (1L), (b) bi-layer (2L), (c) tri-layer (3L), (d) quad-layer (4L), and (e) Bulk 2D HOIPs. The red dash lines indicate the location where the cross-sectional height profiles were taken.

Figure 4 demonstrates the linear dependence between thickness and the number of layers. Thickness of single-layer C4, C8, and C12 was determined to be about 1.76 nm, 2.16 nm, and 2.41 nm, respectively. These values were averaged from at least two flakes in each case and were slightly larger than theoretical values of 2D layered HOIPs [28-32] due to the presence of adhesive residue or molecules absorbed on the surface of the substrate. The

interlayer spacing values of C4, C8, and C12 were estimated to be about 1.4 nm, 1.70 nm, and 2.11 nm, respectively, which are generally consistent with theoretical values.

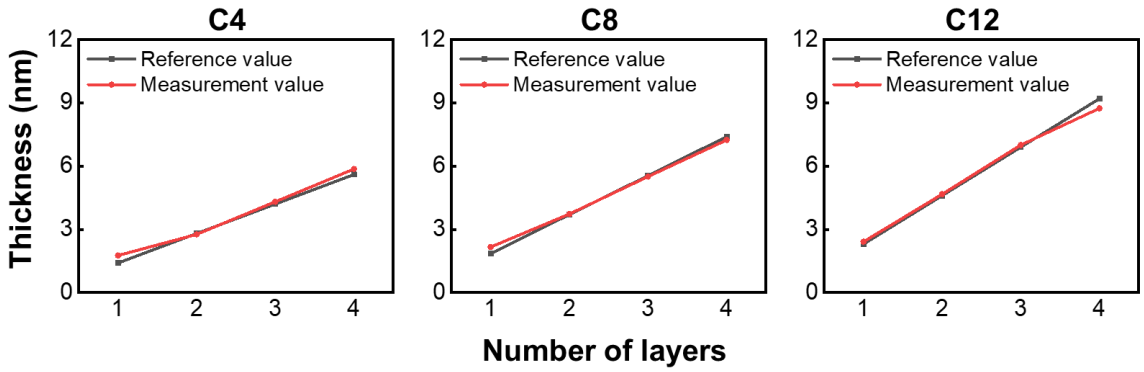

Figure 4. Determination of the number of layers of 2D HOIPs by comparing with reference values [28-32] and measurement values.

2.2. Friction force measurements

Friction characteristics were systematically examined by friction force microscopy (FFM) measurements using an ultra-nanocrystalline diamond (UNCD) tip (ND-CTIR1M-5, NaDiaProbes, Advanced Diamond Technologies) via contact mode. Prior to FFM measurements, the cantilever was calibrated in both normal [33] and lateral [34, 35] directions for the quantitative evaluation of friction force. The force calibration results showed that normal spring constant and lateral force sensitivity were about 0.14 N/m and 0.56 mV/nN, respectively. FFM measurements were performed under various normal forces of 0 nN, 1 nN, 3 nN, 5 nN, 7 nN, and 10 nN in the ambient conditions (28 ℃, 60% RH). It should be noted that 10 nN was chosen as the maximum normal force to reduce the possibility of causing surface damage to atomically thin 2D HOIPs. Moreover, sliding speed was set to 500 nm/s for reliable friction force data considering that the scan length was about 400 nm. In addition, the wear of the AFM tip was indirectly monitored from the variation of the adhesion force [36] determined by force-displacement curve before and after each friction force measurement for the experimental consistency. Furthermore, friction forces were obtained and averaged from two different flakes for each case considering the local variation of friction force and calculated by dividing the differences between trace and retrace value of friction loop by two.

3. RESULTS AND DISCUSSION

3.1. Effect of the organic chain length

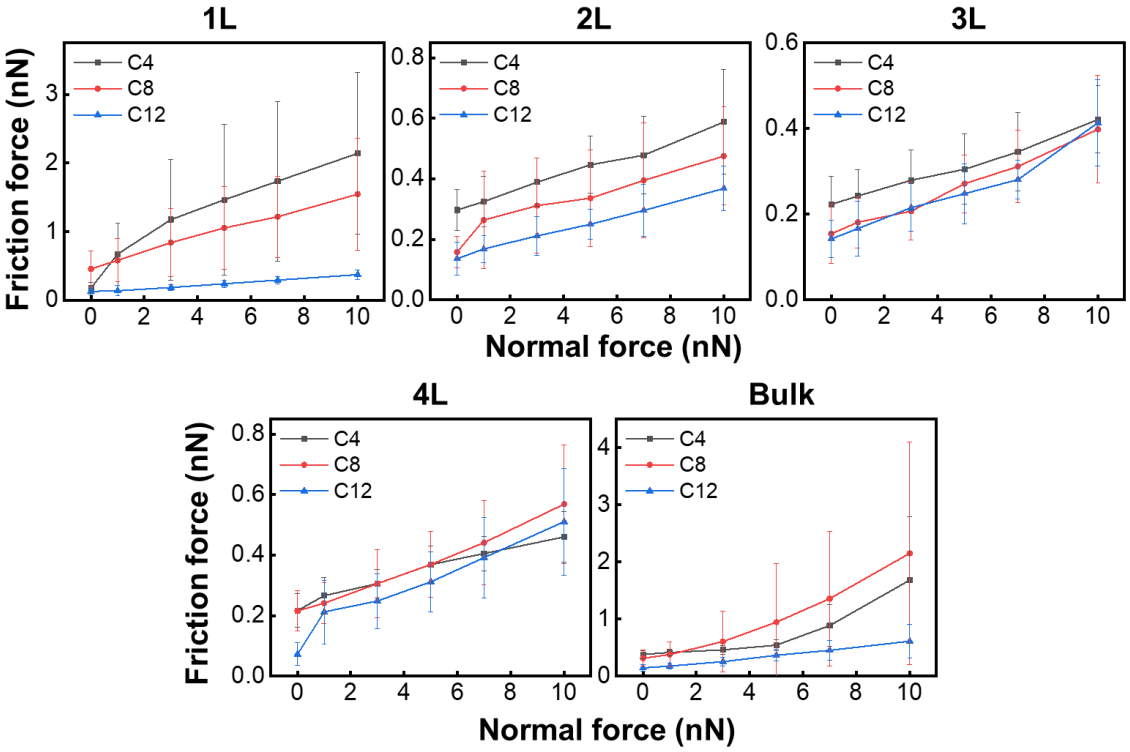

Figure 5. Friction force as a function of normal force of atomically thin 2D HOIPs for the investigation of the effect of the organic chain length.

Figure 5 shows friction force as a function of normal force of atomically thin 2D HOIPs for the investigation of the effect of the organic chain length. For single-layer and bi-layer 2D HOIPs under the same normal force, friction force decreased with increasing the organic chain length from C4 to C12. These results can be explained by the difference in the out-of-plane elastic modulus of 2D HOIPs induced by softening effect. In other words, as the organic chain length increases, the relative amount of the organic part softer than the

inorganic part increases, resulting a decrease in elastic modulus, hence C4 has the highest elastic modulus [17]. Considering that the less compliant materials exhibit more friction [37], it can be expected that the highest friction force of C4 and a decrease in friction force with increasing the organic chain length. However, it is reported that this softening effect due to the increased organic chain length eventually reaches saturation, thus C8 and C12 has similar elastic modulus as shown in figure 6 (a) [17]. Therefore, it is insufficient to account for the larger friction force of C8 than that of C12. A plausible explanation of this outcome is that adhesion force between the AFM tip and C8 was greater than that between the AFM tip and C12, as shown in figure 6 (b), resulting in higher friction force of C8.

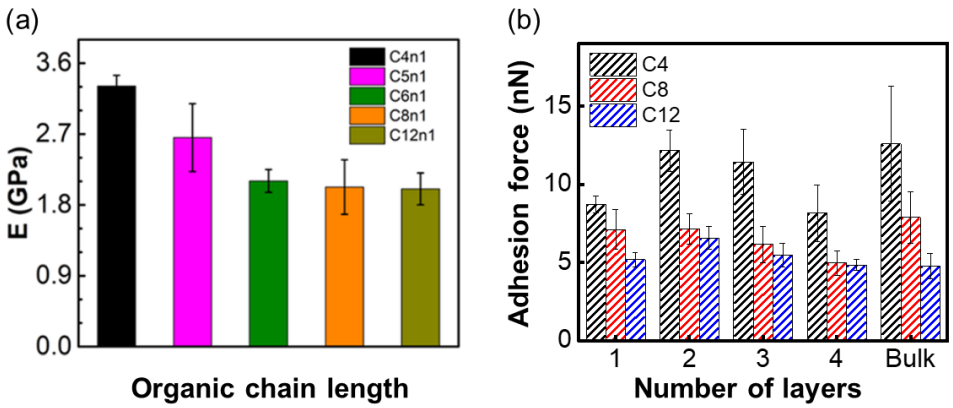

Figure 6. (a) The effect of organic chain length on the out-of-plane elastic modulus [17], (b) Average adhesion forces between the AFM tip and atomically thin 2D HOIPs determined before and after FFM measurements.

Figure 6 (b) shows the average adhesion forces between the AFM tip and atomically thin 2D HOIPs determined at more than 40 locations before and after FFM measurements. Adhesion force decreased with increasing organic chain length, but there was no trend associated with the number of layers. Consequently, the friction characteristics of single-

layer and bi-layer 2D HOIPs were affected by the organic chain length that resulted in differences in elastic modulus and adhesion force.

On the other hand, for tri-layer 2D HOIPs, C8 and C12 showed similar friction force under the same normal force. Particularly, in the case of quad-layer 2D HOIPs, it was hard to find the effect of the organic chain length on friction force, indicating that their dependence on organic chain length becomes less prominent with increasing the number of layers. Additionally, for bulk 2D HOIPs, the greatest friction force of C8 was observed, but this outcome is hard to be considered that friction force was influenced by the organic chain length. Because of the large variation of friction force depending on the location even in the same flake as shown in figure 7 (b), making it difficult to determine the representative friction characteristics of bulk 2D HOIPs. Figure 7 indicates the topography and FFM images of bulk C8 obtained simultaneously during the contact mode scanning using a silicon tip (PPP-LFMR, Nanosensors) for the characterization of the local variation of friction characteristics of bulk 2D HOIPs.

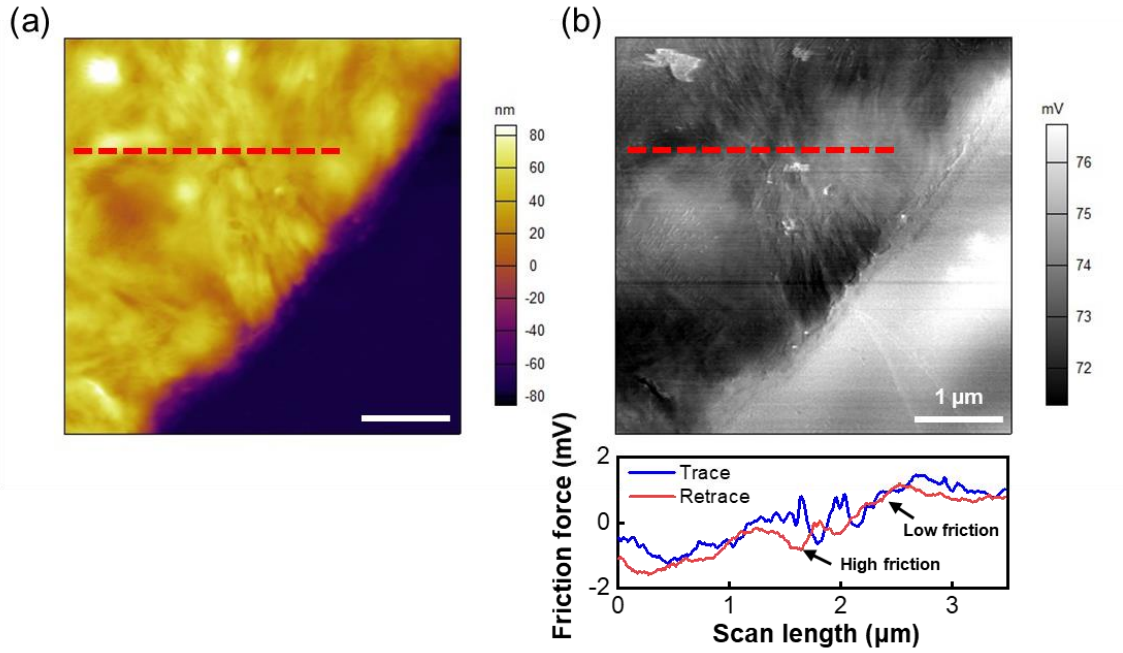

Figure 7. (a) Topography and (b) FFM images of bulk C8. The red dash line indicates the location where the friction loop was taken.

Overall, it is assumed that the effect of the organic chain length on friction becomes less significant as the number of layers increases and other factors such as topography are considered to cause the local variation in the friction characteristics of atomically thin 2D HOIPs.

3.2. Effect of the number of layers

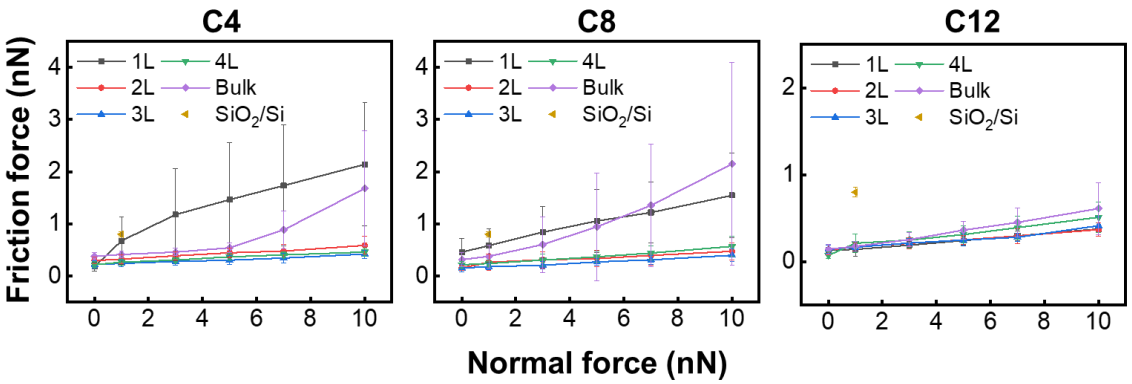

Figure 8. Friction force as a function of a normal force of atomically thin 2D HOIPs for the investigation of the effect of the number of layers.

Figure 8 presents friction force as a function of a normal force of atomically thin 2D HOIPs for the investigation of the effect of the number of layers. Friction force of SiO_2/Si substrate measured under a normal force of 1 nN was also plotted for comparison and was greater than that of 2D HOIPs. Friction forces of C4 and C8 were decreased as the number of layers increased from single-layer to tri-layer and increased with increasing the number of layers from quad-layer. These results may be due to the thickness independence of mechanical properties at large thickness (≥ tri-layer), showing the saturation of the sliding effects [38-40]. Therefore, from quad-layer, the friction characteristics of C4 and C8 were also influenced by other factors other than the number of layers.

In the case of C12, the opposite results of increasing friction force as the number of layers increased were obtained. However, since C12 showed the lowest friction force for all the number of layers compared to C4 and C8, and even the maximum friction force is very

small even less than 0.6 nN, so it can be considered that the effect of the number of layers on friction is less significant for C12.

Thickness dependent friction characteristics were relatively different depending on the type of 2D HOIPs proposed due to their differences in adhesion force induced by the difference in the organic chain length. In general, friction force decreased as the number of layers increased from single-layer to tri-layer. However, the effect of the number of layers was less significant for C12 and all three kinds of bulk 2D HOIPs showed high friction force.

3.3. Effect of topography

Figure 9 (a) and 9 (b) show examples of topographic and FFM images of tri-layer C4, C8, and C12 obtained simultaneously under 5 nN of normal force. It should be noted that FFM images clearly showed the strong correlation between topography and friction force. For the accurate evaluation of the effect of surface slope on the FFM measurements, the cross-sectional height profiles and friction loops were obtained at the same location as shown in figure 9 (c) and 9 (e). For the further investigation of the effect of local slope on friction force, the height derivative was taken from the cross-sectional height profiles, as shown in figure 9 (d). Through the comparison between the surface slope variation and friction force variation, the shapes of height derivative profiles and friction loops were found to be consistent with each other. In other words, the friction force increased and decreased with increasing and decreasing surface slope, respectively. Moreover, high friction force was obtained at the edge with positive slopes and low friction force was observed at the edge with negative slopes. This outcome is may be due to the friction force required for the tip to climb against when the tip encounter a given slope of the topography [41]. Furthermore, topography induced friction forces can be observed by friction force profiles, as shown in figure 9 (f), indicating that the effect of topography on friction could not be eliminated by subtraction of trace and retrace friction force. Based on the friction behaviors according to local slope variation, the effect of topography on nanoscale friction force of atomically thin 2D HOIPs was clearly observed.

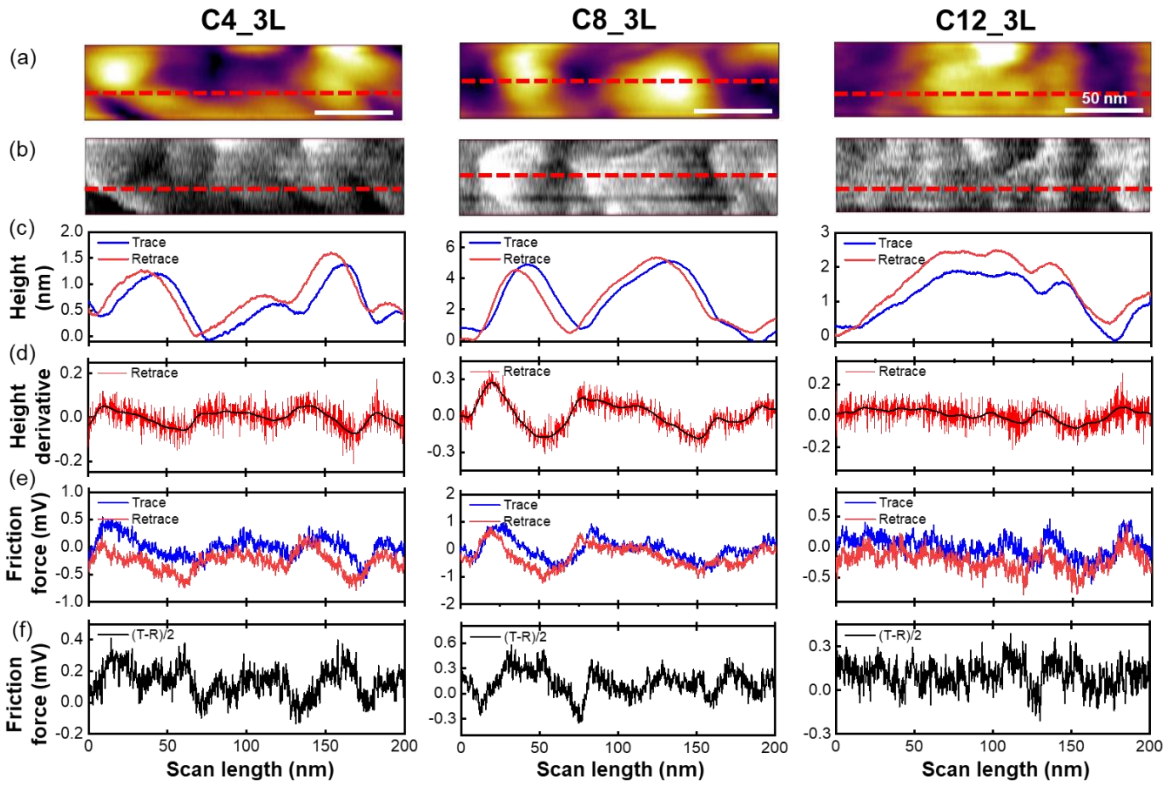

Figure 9. (a) Topographic and (b) FFM images of tri-layer 2D HOIPs obtained simultaneously from the contact mode of AFM under normal force of 5 nN. (c) Cross-sectional height profiles, (d) derivative of cross-sectional height profile, (e) friction loops, and (f) half subtracted friction force are also included. Red dash lines indicate the locations where cross-sectional height profiles, height derivatives and friction loops were taken.

4. CONCLUSIONS AND RECOMMENDATIONS

4.1. Conclusions

In this work, the fundamental friction characteristics of atomically thin 2D HOIPs at the nanoscale were studied. The effect of the organic chain length and the number of layers on friction characteristics were quantitatively investigated. Through the AFM-based approaches, quantitative FFM measurements on single-, bi-, tri-, quad-layer, and bulk 2D HOIPs with three different organic chain length (C4, C8, and C12) were performed.

- Friction force decreased with increasing the organic chain length from C4 to C12 for single-layer and bi-layer. However, it is assumed that the effect of the organic chain length on friction becomes less significant as the number of layers increases.
- Friction force decreased as the number of layers increased from single-layer to tri-layer. However, the effect of the number of layers was less significant for C12 and all three kinds of bulk 2D HOIPs showed high friction force.
- Furthermore, the effect of topography on nanoscale friction force of atomically thin 2D HOIPs was clearly observed based on the friction behaviors according to local slope variation.

4.2. Recommendations for future works

- For bulk 2D HOIPs, aging could be expected from the changes in topography and thickness as shown in figure 10. Therefore, a systematic research is needed to investigate the effect of the aging on the friction characteristics for the stability in application.

- Damaged single-layer C4 was observed as shown in figure 11, showing the increased friction force under 15 nN of normal force. Thus, the study of wear characteristics of 2D HOIPs will allow a better understanding of tribological characteristics.

- As inorganic layers have a greater influence on mechanical properties of 2D HOIPs than organic layers do [17, 38], the study on the effect of thickness of the inorganic layer on friction characteristics is needed. So the tunability of friction characteristics of 2D HOIPs will be broadened by controlling the inorganic layer as well as the organic chain length and number of layers.

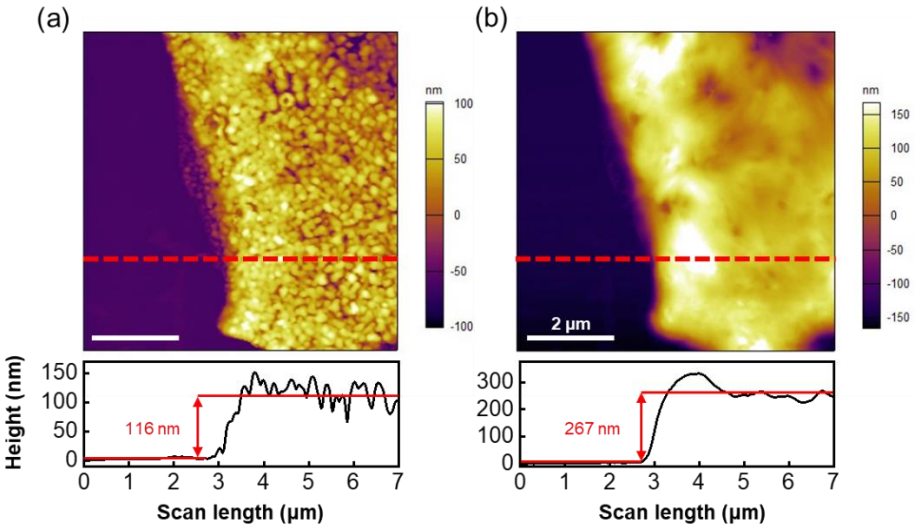

Figure 10. Topographic images and cross-sectional height profiles of bulk C4 (a) before and (b) after aging. Red dash lines indicate the locations where cross-sectional height profiles were taken.

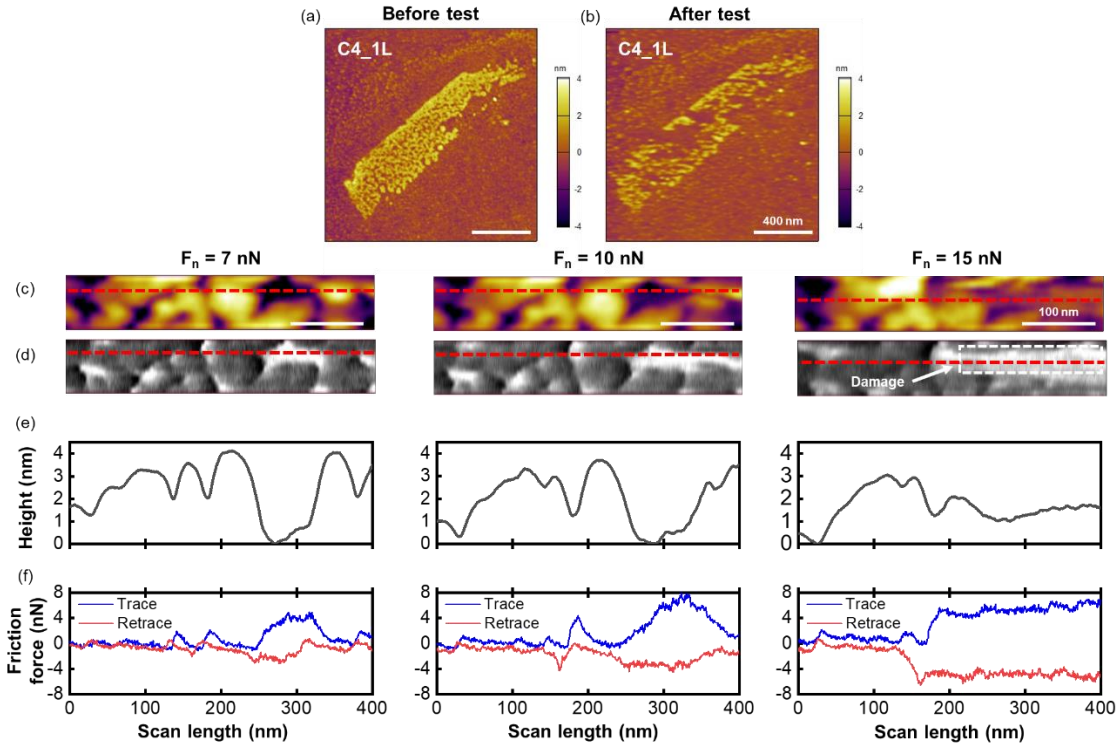

Figure 11. Topographic images of single-layer C4 (a) before and (b) after test. And (c) topographic and (d) FFM images of single-layer C4 obtained simultaneously from the contact mode of AFM. (e) Cross-sectional height profiles and (f) friction loops were taken from the red dash lines.

REFERENCES

[1] Green, M. A.; Hishikawa, Y.; Dunlop, E. D.; Levi, D. H.; Hohl-Ebinger, J.; Yoshita, M.; Ho-Baillie, A. W. Y., Solar Cell Efficiency Tables (Version 53). *Prog.Photovoltaics* **2019,** *27*, 3-12.

[2] Tu, Q.; Spanopoulos, I.; Vasileiadou, E. S.; Li, X.; Kanatzidis, M. G.; Shekhawat, G. S.; Dravid, V. P., Exploring the Factors Affecting the Mechanical Properties of 2D Hybrid Organic-Inorganic Perovskites. *ACS Appl Mater Interfaces* **2020,** *12* (18), 20440-20447.

[3] Snaith, H. J., Perovskites: The Emergence of a New Era for Low-Cost, High-Efficiency Solar Cells. *The Journal of Physical Chemistry Letters* **2013,** *4* (21), 3623-3630.

[4] Eperon, G. E.; Stranks, S. D.; Menelaou, C.; Johnston, M. B.; Herz, L. M.; Snaith, H. J., Formamidinium lead trihalide: a broadly tunable perovskite for efficient planar heterojunction solar cells. *Energy & Environmental Science* **2014,** *7* (3).

[5] Tu, Q.; Spanopoulos, I.; Hao, S.; Wolverton, C.; Kanatzidis, M. G.; Shekhawat, G. S.; Dravid, V. P., Probing Strain-Induced Band Gap Modulation in 2D Hybrid Organic–Inorganic Perovskites. *ACS Energy Letters* **2019,** *4* (3), 796-802.

[6] Choi, J.; Han, J. S.; Hong, K.; Kim, S. Y.; Jang, H. W., Organic-Inorganic Hybrid Halide Perovskites for Memories, Transistors, and Artificial Synapses. *Adv Mater* **2018,** *30* (42), e1704002.

[7] Skinner, S. J., Recent advances in Perovskite-type materials for solid oxide fuel cell cathodes. *Int J Inorg Mater* **2001,** *3* (2), 113-121.

[8] Gu, C.; Lee, J. S., Flexible Hybrid Organic-Inorganic Perovskite Memory. *ACS Nano* **2016,** *10* (5), 5413-8.

[9] Murali, B.; Saidaminov, M. I.; Abdelhady, A. L.; Peng, W.; Liu, J.; Pan, J.; Bakr, O. M.; Mohammed, O. F., Robust and air-stable sandwiched organo-lead halide perovskites for photodetector applications. *Journal of Materials Chemistry C* **2016,** *4* (13), 2545-2552.

[10] Berhe, T. A.; Su, W.-N.; Chen, C.-H.; Pan, C.-J.; Cheng, J.-H.; Chen, H.-M.; Tsai, M.-C.; Chen, L.-Y.; Dubale, A. A.; Hwang, B.-J., Organometal halide perovskite solar cells: degradation and stability. *Energy & Environmental Science* **2016,** *9* (2), 323-356.

[11] Fang, H.-H.; Yang, J.; Tao, S.; Adjokatse, S.; Kamminga, M. E.; Ye, J.; Blake, G. R.; Even, J.; Loi, M. A., Unravelling Light-Induced Degradation of Layered Perovskite Crystals and Design of Efficient Encapsulation for Improved Photostability. *Advanced Functional Materials* **2018,** *28* (21).

[12] Niu, G.; Guo, X.; Wang, L., Review of recent progress in chemical stability of perovskite solar cells. *Journal of Materials Chemistry A* **2015,** *3* (17), 8970-8980.

[13] Saparov, B.; Mitzi, D. B., Organic-Inorganic Perovskites: Structural Versatility for Functional Materials Design. *Chem Rev* **2016,** *116* (7), 4558-96.

[14] Ruddlesden, S. N.; Popper, P., New Compounds of the K2NIF4 type. *Acta Crystallogr B* **1957,** *10*, 538−539.

[15] Ruddlesden, S. N.; Popper, P., The Compound Sr3Ti2O7 and Its Structure. *Acta Crystallogr B* **1958,** *11*, 54−55.

[16] Schaak, R. E.; Mallouk, T. E., Perovskites by Design: A Toolbox of Solid-State Reactions. *Chem. Mater.* **2002,** *14*, 1455−1471.

[17] Tu, Q.; Spanopoulos, I.; Hao, S.; Wolverton, C.; Kanatzidis, M. G.; Shekhawat, G. S.; Dravid, V. P., Out-of-Plane Mechanical Properties of 2D Hybrid Organic-Inorganic Perovskites by Nanoindentation. *ACS Appl Mater Interfaces* **2018,** *10* (26), 22167-22173.

[18] Wang, Z. L., Triboelectric Nanogenerators as New nanogenerators as new energy technology and as active mechanical and chemical sensors. *ACS nano* **2013,** *7* (11), 9533-9557.

[19] Su, L.; Zhao, Z.; Li, H.; Wang, Y.; Kuang, S.; Cao, G.; Wang, Z.; Zhu, G., Photoinduced enhancement of a triboelectric nanogenerator based on an organolead halide perovskite. *Journal of Materials Chemistry C* **2016,** *4* (43), 10395-10399.

[20] Lv, Y.; Song, X.; Yin, Y.; Feng, Y.; Ma, H.; Hao, C.; Jin, S.; Shi, Y., Hexylammonium Iodide Derived Two-Dimensional Perovskite as Interfacial Passivation Layer in Efficient Two-Dimensional/Three-Dimensional Perovskite Solar Cells. *ACS Appl Mater Interfaces* **2020,** *12* (1), 698-705.

[21] Filleter, T.; McChesney, J. L.; Bostwick, A.; Rotenberg, E.; Emtsev, K. V.; Seyller, T.; Horn, K.; Bennewitz, R., Friction and dissipation in epitaxial graphene films. *Phys Rev Lett* **2009,** *102* (8), 086102.

[22] Lee, C.; Li, Q.; Kalb, W.; Liu, X. Z.; Berger, H.; Carpick, R. W.; Hone, J., Frictional characteristics of atomically thin sheets. *Science* **2010,** *328* (5974), 76-80.

[23] Fang, L.; Liu, D. M.; Guo, Y.; Liao, Z. M.; Luo, J. B.; Wen, S. Z., Thickness dependent friction on few-layer MoS2, WS2, and WSe2. *Nanotechnology* **2017,** *28* (24), 245703.

[24] Li, Q.; Lee, C.; Carpick, R. W.; Hone, J., Substrate effect on thickness-dependent friction on graphene. *physica status solidi (b)* **2010,** *247* (11-12), 2909-2914.

[25] Cho, D. H.; Wang, L.; Kim, J. S.; Lee, G. H.; Kim, E. S.; Lee, S.; Lee, S. Y.; Hone, J.; Lee, C., Effect of surface morphology on friction of graphene on various substrates. *Nanoscale* **2013,** *5* (7), 3063-9.

[26] Novoselov, K. S.; Geim, A. K.; Morozov, S. V.; Jiang, D.; Zhang, Y.; Dubonos, S. V.; Grigorieva, I. V.; Firsov, A. A., Electric Field Effect in Atomically Thin Carbon Films. *Science* **2004,** *306*, 666-669.

[27] Niu, W.; Eiden, A.; Vijaya Prakash, G.; Baumberg, J. J., Exfoliation of self-assembled 2D organic-inorganic perovskite semiconductors. *Applied Physics Letters* **2014,** *104*, 171111.

[28] Billing, D. G.; Lemmerer, A., Synthesis, characterization and phase transitions in the inorganic-organic layered perovskite-type hybrids [(CnH2n+1NH3)2PbI4], n = 4, 5 and 6. *Acta Crystallogr B* **2007,** *63* (Pt 5), 735-47.

[29] Billing, D. G.; Lemmerer, A., Synthesis, characterization and phase transitions of the inorganic–organic layered perovskite-type hybrids [(CnH2n+1NH3)2PbI4] (n = 12, 14, 16 and 18). *New Journal of Chemistry* **2008,** *32* (10).

[30] Lemmerer, A.; Billing, D. G., Synthesis, characterization and phase transitions of the inorganic-organic layered perovskite-type hybrids [(C(n)H(2n+1)NH3)2PbI4], n = 7, 8, 9 and 10. *Dalton Trans* **2012,** *41* (4), 1146-57.

[31] Pradeesh, K.; Baumberg, J. J.; Prakash, G. V., In situ intercalation strategies for device-quality hybrid inorganic-organic self-assembled quantum wells. *Applied Physics Letters* **2009,** *95* (3).

[32] Stoumpos, C. C.; Cao, D. H.; Clark, D. J.; Young, J.; Rondinelli, J. M.; Jang, J. I.; Hupp, J. T.; Kanatzidis, M. G., Ruddlesden–Popper Hybrid Lead Iodide Perovskite 2D Homologous Semiconductors. *Chemistry of Materials* **2016,** *28* (8), 2852-2867.

[33] Hutter, J. L.; Bechhoefer, J., Calibration of atomic-force microscope tips. *Review of Scientific Instruments* **1993,** *64* (7), 1868-1873.

[34] Chung, K. H.; Reitsma, M. G., Lateral force microscope calibration using multiple location pivot loading of rectangular cantilevers. *Rev Sci Instrum* **2010,** *81* (2), 026104.

[35] Tran Khac, B. C.; Chung, K. H., Quantitative assessment of contact and non-contact lateral force calibration methods for atomic force microscopy. *Ultramicroscopy* **2016,** *161*, 41-50.

[36] Gotsmann, B.; Lantz, M. A., Atomistic wear in a single asperity sliding contact. *Phys Rev Lett* **2008,** *101* (12), 125501.

[37] Kwon, S.; Ko, J. H.; Jeon, K. J.; Kim, Y. H.; Park, J. Y., Enhanced nanoscale friction on fluorinated graphene. *Nano Lett* **2012,** *12* (12), 6043-8.

[38] Tu, Q.; Spanopoulos, I.; Yasaei, P.; Stoumpos, C. C.; Kanatzidis, M. G.; Shekhawat, G. S.; Dravid, V. P., Stretching and Breaking of Ultrathin 2D Hybrid Organic-Inorganic Perovskites. *ACS Nano* **2018,** *12* (10), 10347-10354.

[39] Wei, Q.; Peng, X., Superior mechanical flexibility of phosphorene and few-layer black phosphorus. *Applied Physics Letters* **2014,** *104* (25).

[40] Wei, X.; Meng, Z.; Ruiz, L.; Xia, W.; Lee, C.; Kysar, J. W.; Hone, J. C.; Keten, S.; Espinosa, H. D., Recoverable Slippage Mechanism in Multilayer Graphene Leads to Repeatable Energy Dissipation. *ACS Nano* **2016,** *10* (2), 1820-8.

[41] Sundararajan, S.; Bhushan, B., Topography-induced contributions to friction forces measured using an atomic force/friction force microscope. *Journal of Applied Physics* **2000,** *88* (8).